PCCP

Insights of the Peroxychloroformyl Radical ClC(O)OO via Microwave Spectrum

Journal:	*Physical Chemistry Chemical Physics*
Manuscript ID	CP-ART-09-2024-003506.R1
Article Type:	Paper
Date Submitted by the Author:	18-Oct-2024
Complete List of Authors:	Chang, Ching Hua; National Yang Ming Chiao Tung University Chao, Wen; California Institute of Technology, Tsai, Cheng-Han; National Yang Ming Chiao Tung University, Applied Chemistry Okumura, Mitchio; California Institute of Technology Winiberg, Frank; Jet Propulsion Laboratory Endo, Yasuki; National Yang Ming Chiao Tung University, APPLIED CHEMISTRY

Insights of the Peroxychloroformyl Radical ClC(O)OO via Microwave Spectrum

Ching-Hua Chang,[1] Wen Chao,[2] Cheng-Han Tsai,[1] Mitchio Okumura,[2] Frank A. F. Winiberg,[3] and Yasuki Endo[1,*]

[1] *Department of Applied Chemistry, Science Building II, National Yang Ming Chiao Tung University, 1001 Ta-Hsueh Rd., Hsinchu 30093, Taiwan*

[2] *Division of Chemistry and Chemical Engineering, California Institute of Technology, 1200 E California Blvd, Pasadena, CA 91125 United States*

[3] *Jet Propulsion Laboratory, California Institute of Technology, 4800 Oak Grove Drive, Pasadena, CA 91109-8099, United States*

*Author to whom correspondence should be addressed.
Electric mail: endo@nycu.edu.tw

Abstract

The exploration of Venus has received much attention in the past and will keep growing due to the starting of the NASA DAVINCI project. To explain the extremely low O_2:CO ratio observed in Venus' atmosphere, a chlorine-initiated CO oxidation catalytic cycle has been proposed. However, relevant studies on the key intermediates, such as the peroxychloroformyl radical (ClC(O)OO), are rare. In this study, the ClC(O)OO radical was observed using Fourier-Transform Microwave (FTMW) spectroscopy under the supersonic expansion condition. Two conformers, *trans*-ClC(O)OO and *cis*-ClC(O)OO, and their chlorine isotopologues were detected. The molecular constants including the fine and hyperfine constants, were determined. Based on the experimental and the *ab initio* calculations, the unpaired electron is mostly located at the terminal oxygen atom, supported by the small magnetic hyperfine constants of chlorine. In addition, the angles between the Cl–C bond and the *a*-axis of the *trans*-^{35}ClC(O)OO and *trans*-^{37}ClC(O)OO are similar, but these angles are different for *cis*-ClC(O)OO, making the quadrupole coupling tensors in the inertial axes disagree with the ratio of the quadrupole moments of ^{35}Cl and ^{37}Cl. Finally, we concluded that the ClC(O)OO radicals should behave similarly to other peroxyl radicals, as assumed in the current photochemical model of Venus.

Introduction

As one of the nearest planets from the Earth, observations of Venus have been ongoing for more than hundreds of years, from spectroscopic measurements by eye and telescope to physical probing by sending orbiters and probes that reach the Venusian atmosphere and surface.[1] An understanding of the evolution of Venus in our solar system could help to elucidate the formation of exoplanetary systems and the habitability of exoplanets.[2] The current atmospheric composition provides essential information to verify photochemical models of the Venusian atmosphere and to trace back its history.[3] However, puzzles remain,[4] leading to significant gaps between the results of model simulations and real-world observations.

Venus' atmosphere consists of 96.5% CO_2, 3.5% N_2 and trace amounts of CO, H_2O, Ar, SO_2 and HCl.[1, 5] The extremely low O_2 level (< 3 ppm)[6] contrasts with the observations of O_2 night glow of the $A^1\Delta_g$-$X^3\Sigma_g^-$ transition.[7] The O_2 molecules, produced from the photolysis of CO_2 to generate O atoms and the subsequent oxygen atom recombination ($CO_2 + h\nu \rightarrow CO + O$; $O + O + M \rightarrow O_2^* + M$), could accumulate in the Venus mesosphere.

A chlorine atom initiated catalytic cycle of CO oxidation has been proposed to explain the low [O_2] and [CO], and the high [CO_2] through the formation of the chloroformyl radicals (ClCO, R1) and the peroxychloroformyl radical (ClC(O)OO, R2).[8] The ClC(O)OO radical could react with either O atoms (R3) or itself (R4) to form CO_2 and O_2, releasing Cl atoms to complete the catalytic cycle (R3a and R4a).[9] However, the CO_2/ClO product channels (R3b and R4b) reduces the active Cl atom concentration and are estimated to contribute as much of a chlorine reservoir as HCl,[10] decreasing the efficiency of the Cl catalytic effect.

Cl + CO	→	ClCO	(R1a)
ClCO	→	Cl + CO	(R1b)
ClCO + O_2	→	ClC(O)OO	(R2)
O + ClC(O)OO	→	Cl + CO_2 + O_2	(R3a)
	→	ClO + CO_2 + O	(R3b)
2 ClC(O)OO	→	2 Cl + 2 CO_2 + O_2	(R4a)
	→	2 ClO + 2 CO_2	(R4b)

To accurately model the Cl catalytic effect of CO oxidation, critical parameters including the ClCO equilibrium constant, the ClCO + O_2 reaction rate coefficient, the reaction rate coefficients involving ClC(O)OO and the product branching ratios, are necessary. However, relevant kinetic studies are sparse. Current Venus photochemical models estimate these parameters by adopting the values of their isoelectronic analogs,[5, 11] *e.g.* ClSO by ClOO and ClC(O)OO by FC(O)OO, but recent results from the pure rotational spectrum of ClSO radicals have shown that the reactivities of ClOO and ClSO

are significantly different.[12]

In addition to kinetic data, spectroscopic measurements can provide hints to evaluate the reliability of the rate coefficients and the product branching ratio in model simulations. For the ClC(O)OO radical, Francisco and Williams[13] investigated the ground and the first excited state *via ab initio* calculations and predicted the X^2A'' ground state character at the UHF/6-31G** level. Pernice *et al.*[14] generated the ClC(O)OO radicals from pyrolysis of $ClC(O)OONO_2$ and recorded infrared (IR) and UV-Vis spectra in Ar, Ne and O_2 matrices. Recently, Bahera and Lee reported the gas phase IR spectrum of the ClC(O)OO radicals.[15] They pointed out that the O–O stretching frequency is about 1100 cm^{-1}, similar to those of other peroxyl radicals.

The reactivity of the ClC(O)OO radical strongly depends on the distribution of the unpaired electron, *i.e.* the shape of the singly occupied molecular orbital (SOMO). High resolution spectroscopic measurements can provide the fine and hyperfine structure constants that elucidate the location of the unpaired electron. In this work, we investigated the high resolution pure rotational spectrum of the ClC(O)OO radical in the frequency range of 4 – 40 GHz using a Fourier-transform microwave (FTMW) spectrometer. The fine and hyperfine structures were analyzed to obtain molecular constants involving the unpaired electron spin and the nuclear spin of the chlorine atom. High level *ab initio* calculations were conducted for comparison, and insights obtained from the molecular constants were discussed.

Quantum Chemical Calculations

The ClC(O)OO radical is considered to have two conformers, *trans*-ClC(O)OO and *cis*-ClC(O)OO, depending on the direction of terminal OO. Geometries of the two conformers were optimized using the Molpro program package at the RCCSD(T)-F12A/cc-pVTZ-f12 level of theory.[16] Their optimized structures are shown in **Fig. 1**. The calculated molecular constants and dipole moments are summarized in **Table 1**.

As shown in **Fig. 2**, the energy of *trans*-^{35}ClC(O)OO is 4.4 kJ mol^{-1} lower than that of *cis*-^{35}ClC(O)OO with a barrier between both conformers about 22 kJ mol^{-1} by calculations at the RCCSD(T)/cc-pVTZ level of theory. The energy difference is 2.65 kJ mol^{-1} at the RCCSD(T)-F12A/cc-pVTZ-f12 level of theory with the zero-point energy correction at the RCCSD(T)/cc-pVTZ level of theory. This barrier indicates that the interconversion between the *trans*- and *cis*- conformers is slow below room temperature, and the two conformers may therefore be observed. Indeed, the FTIR measurements under gas-phase flow cell conditions at 298 K have identified these two

conformers from the photolysis of the $(ClCO)_2/N_2/O_2$ mixtures.[15]

For *trans*-^{35}ClC(O)OO, the dipole moment along the *a*-axis (μ_a = 0.91 Debye) is close to that along the *b*-axis (μ_b =1.13 Debye). In contrast, for *cis*-^{35}ClC(O)OO, the μ_a (0.27 Debye) is a factor of six smaller than the μ_b (1.83 Debye). Larger microwave power is required to polarize the *a*-type transitions of *cis*-^{35}ClC(O)OO relative to the *b*-type transitions. The calculated rotational constants are A_e = 9899.3 MHz, B_e = 2871.9 MHz, and C_e = 2226.1 MHz for *trans*-^{35}ClC(O)OO, indicating that the *trans* conformer is close to a prolate top molecule ($A > B \approx C$, $\kappa = -0.83$). On the other hand, the rotational constants of *cis*-^{35}ClC(O)OO are A_e = 5629.7 MHz, B_e = 4406.7 MHz, and C_e = 2471.8 MHz and the geometry is close to an oblate top molecule ($A \approx B > C$, κ = 0.22). The fine and hyperfine parameters required to assign the lines observed in this experiment were calculated using the Gaussian 16 program package.[17] The calculations were carried out at the B3LYP/aug-cc-pVTZ level of theory at the geometry optimized by the Molpro program package.[16]

The molecular constants of ^{37}ClC(O)OO were calculated using the same method as that of ^{35}ClC(O)OO. It is important to properly scale the calculated molecular constants of the ^{37}Cl isotopologues to obtain accurate predictions since the intensities of the spectral lines are a factor of three weaker than those for the ^{35}Cl isotopologue due to their natural abundances. The magnetic hyperfine constants and the quadrupole coupling constants were scaled using the ratios of the magnetic moments and the quadrupole moments of ^{35}Cl and ^{37}Cl.[18] The scaled parameters for ^{37}ClC(O)OO are shown in **Table 2**.

Experimental Methods

The ClC(O)OO radical was investigated using FTMW spectroscopy, which has been described in detail previously.[19] The operating frequency of the spectrometer is 4–40 GHz. In brief , a gas mixture with 0.2% CCl_4, 2% CO, and 2% O_2 diluted in Ne was flowed into the cavity as a supersonic expansion through a pulsed-solenoid valve, and its rotational temperature was cooled down to nearly 2.5 K with a backing pressure of 3 atm. After the exit of the valve, the gas passed through two electrodes, separated by a boron nitride insulator, where the ClC(O)OO radical was generated by a pulsed electronic discharge (~1.2 kV). The discharge nozzle was located at the center of one of the Fabry-Perot cavity mirrors, where the outer electrode is exposed on the mirror surface. During the experiment, the pressure of the vacuum chamber was about 8×10^{-5} Torr. The microwave pulse was sent into the cavity and polarized the radical through rotational electric resonances. The microwave pulse, generated by a primary

synthesizer (Rohde & Schwarz, SMB 100A, 1 – 40 GHz) was emitted into the cavity by an antenna located at the center of the mirror opposite to the discharge nozzle.

In this setup, the jet propagates along parallel and anti-parallel components of the microwave standing wave field in the cavity, resulting in the Doppler doubling for a transition line as shown in **Fig. 3**. The free induction decay signal emitted from the polarized radical was detected by the same antenna emitting the polarizing microwave pulse. A duration of 0.3 μs was required for the microwave pulse to detect the *trans*-ClC(O)OO radical. However, about 0.7 μs of duration was required to detect *a*-type transitions of the *cis*-ClC(O)OO radical because of its small μ_a. Three sets of Helmholtz coils were utilized in the experiments to compensate the Earth's magnetic field avoiding the energy level splitting of open-shell species due to the Zeeman effect.

Analysis

The Hamiltonian, $\mathbf{H} = \mathbf{H}_{rot} + \mathbf{H}_{cd} + \mathbf{H}_{nsr} + \mathbf{H}_{sr} + \mathbf{H}_{hf} + \mathbf{H}_{Q}$, was used to analyze the transition frequencies of the ClC(O)OO radical. The $\mathbf{H}_{rot}$ denotes the rotational Hamiltonian. The $\mathbf{H}_{sr}$, $\mathbf{H}_{hf}$, and $\mathbf{H}_{Q}$ denote the electron spin-rotation interaction term ($\varepsilon_{\alpha\beta}$), the magnetic hyperfine term (a_F and $\boldsymbol{T}$), and the nuclear quadrupole coupling term ($\chi_{\alpha\beta}$), respectively. In addition to the fine and hyperfine interactions, minor corrections (magnitude in a few kHz) from the centrifugal distortion term, $\mathbf{H}_{cd}$ in Watson's A-reduced form (Δ_N, Δ_{NK}, Δ_K, δ_N and δ_K), and the nuclear spin-rotation interaction term, $\mathbf{H}_{nsr}$ ($C_{\alpha\alpha}$), were considered.

For a non-linear molecule, the orbital angular momentum, **L**, is usually quenched, leaving the electron spin-rotation interaction, $\mathbf{H}_{sr}$, the most pronounced factor for the fine structure. The Hund's case (b) formula was used to analyze the fine structure. In this approximation, the total angular momentum, **J**, can be expressed as $\mathbf{J} = \mathbf{N} + \mathbf{S}$, where **N** denotes the sum of the rotational angular momentum and the orbital angular momentum, and **S** denotes the electron spin angular momentum. The magnitude of the electron spin-rotation constants ranges from a few tens of MHz to hundreds of MHz.

The interactions involving the nuclear spin angular momentum, **I**, result in the hyperfine structures. Due to the lack of the orbital angular momentum, we can ignore the interaction between **L** and **I**. On the other hand, the magnetic hyperfine interaction between **S** and **I** have to be considered and can be expressed as

$$\mathbf{H}_{hf} = a_F \mathbf{I} \cdot \mathbf{S} + \mathbf{I} \cdot \mathbf{T} \cdot \mathbf{S}, \qquad \mathbf{T} = \begin{bmatrix} T_{aa} & T_{ab} & 0 \\ T_{ba} & T_{bb} & 0 \\ 0 & 0 & T_{cc} \end{bmatrix},$$

where **T** denotes a second-rank traceless tensor with three independent components for planar radicals, and a_F is the Fermi contact interaction constant. The total angular momentum including the nuclear spin angular momentum, **F**, is written as **F** = **J** + **I**. For the ClC(O)OO radicals, S = 1/2 and I(Cl) = 3/2; thus, each rotational level splits into 8 fine and hyperfine levels for most of the cases.

Results

Tests of the Gas Mixture Recipes

To detect the ClC(O)OO transitions, we tried a few different recipes for optimizing the *a*-type transition lines of the ClCO radical.[20] Initially, a gas mixture with 10% of O_2 (0.2% CCl_4, 2% CO) was tested. We observed very strong signals of the ClOO radical and the ClCO signals were hardly detected. Although the Cl-CO bond energy (ΔH_{Cl+CO}(0K) = 28 ± 3 kJ mol^{-1})[21] is larger than the Cl-OO bond energy (ΔH_{Cl+OO}(0K) =19.6 ± 0.42 kJ mol^{-1})[22] and the energy of ClC(O)OO is about 138 kJ mol^{-1} lower than that of ClOO + CO, most of the Cl atoms react with O_2 and the ClC(O)OO radical is hardly formed. We also tested the gas mixture of CCl_4:CO:O_2 = 0.3%:2%:1% in Ne. As expected, we observed stronger ClCO signals and much weaker ClOO signals. In addition, the ClC(O)OO signals were observed for this mixture. Eventually, the gas mixture of 0.3% of CCl_4, 2% of CO, and 2% of O_2 balanced with Ne to 10 atm was used to get the optimized ClC(O)OO signals.

Microwave Spectral Measurements

We first searched for the *a*-type transitions for the *trans*-ClC(O)OO radical. Usually, the prediction of the K_a = 0 *a*-type transitions is more accurate than other transitions since the *B* and *C* rotational constants contribute the most. The calculated B_e and C_e rotational constants are slightly (~ some tens MHz) larger than the measured values because the vibrationally averaged bond lengths are longer than the equilibrium bond lengths. By assigning the *a*-type transitions, better estimations of the *B* and *C* rotational constants and improved predictions of the *b*-type transition frequencies were obtained. For the *cis*-ClC(O)OO radicals, *b*-type transitions were searched for first since the calculated dipole moment μ_a is small. In this case we had to scan a wider region to detect the lines of *cis*-ClC(O)OO.

Fig. 3 shows the *a*-type 4_{04}-3_{03} transition of the *trans*-^{35}ClC(O)OO radical. The observed fine and hyperfine patterns agreed with the predictions being observed at

transition frequencies roughly 70 MHz lower. Intensities were usually stronger using Ne as the carrier gas than the intensities using Ar. For example, the 4_{04}-3_{03} transition of *trans*-^{35}ClC(O)OO was too weak to be observed when Ar was used as a carrier gas.

For the *cis*-ClC(O)OO radical, one *a*-type transition and two *b*-type transitions were observed in the 22190 – 22230 GHz window as shown in **Fig. 4**. Intensities of the 4_{04}-3_{03} and 2_{20}-1_{11} transitions have different responses to the duration of the polarizing microwave pulse since $|\mu_b|$ is about a factor of six larger than $|\mu_a|$. The transitions were assigned by comparing the predicted hyperfine patterns and the power dependence of each line. The relative intensities of the 4_{14}-3_{03} hyperfine components agreed with the predicted pattern. However, the absolute intensities were larger than the 2_{20}-1_{11} transition. This discrepancy was probably caused by the instability of the experimental conditions since they were observed on different days.

We observed a total of 14 *a*-type and 8 *b*-type transitions (123 hyperfine components) for *trans*-^{35}ClC(O)OO, and 10 *a*-type and 6 *b*-type transitions (116 hyperfine components) for *cis*-^{35}ClC(O)OO. These sets of data allowed us to determine totals of 17 and 18 molecular constants for *trans*-^{35}ClC(O)OO and *cis*-^{35}ClC(O)OO, respectively, where a few centrifugal distortion and nuclear spin-rotation constants were fixed to the calculated values in the fitting.

The pure rotational transitions for ^{37}ClC(O)OO were also searched for. The calculated rotational constants of ^{37}ClC(O)OO were scaled, based on the ratio of the calculated and measured ^{35}ClC(O)OO rotational constants, for predicting the initial hyperfine transition frequencies. The observed fine and hyperfine structures for both *trans*-^{37}ClC(O)OO and *cis*-^{37}ClC(O)OO were similar to ^{35}ClC(O)OO as expected. The relative intensities for ^{35}ClC(O)OO and ^{37}ClC(O)OO followed the 3:1 natural abundance ratio of the chlorine atoms. Due to the small signal intensities, only 43 and 57 hyperfine components were observed for *trans*-^{37}ClC(O)OO and *cis*-^{37}ClC(O)OO, respectively. The determined molecular constants are summarized in **Table 1** and **Table 2**, and the observed transitions frequencies are summarized in **Tables S1-S4**.

Discussions

In this study, two conformers of the ClC(O)OO radical and their chlorine isotopologues were observed by detecting their pure rotational transitions in a supersonic expansion of a gas mixture containing CCl_4, CO and O_2 diluted in Ne, from a discharge nozzle. Both *cis*-ClC(O)OO and *trans*-ClC(O)OO conformers were observed with similar intensities. This observation agrees with the insights obtained

from the *ab initio* calculations. First, the energy barrier between the *cis*- and *trans*-conformers is indeed about ten times larger than the thermal energy at 298 K, and, therefore, the interconversion is slow below the room temperature. Second, both conformers have similar stability since the energy of *trans*-^{35}ClC(O)OO is only 2.65 kJ mol^{-1} lower than the energy of *cis*-^{35}ClC(O)OO. Although the rotational temperature in the jet is only about 2.5 K, the two conformers are produced at much higher temperature. Both of the conformers are thus produced almost equally, and the population ratio is preserved even when they are cooled in the supersonic expansion.

The Electron Spin-Rotation Constants

As shown in **Fig. 5** calculations predict that the unpaired electrons of the two conformers occupy the out-of-plane p_c orbital of the terminal oxygen with the ^2A" electronic ground states. Since the electron spin-rotation interaction is a second order term, the perturbational approach by the second order correction indicates that the first excited state contributes the most. For both conformers, the first excited state corresponds to a transition of the beta electron from the in-plane *p* orbital to the out-of-plane p_c orbital, corresponding to the negative ε_{aa} as shown in **Table 1**.

For the *trans*-ClC(O)OO, the direction of the orbital angular momentum produced by the electron excitation is almost parallel to the *a*-axis, resulting in a large contribution to the *a*-axis components for the spin-rotation interaction. On the other hand, for *cis*-ClC(O)OO, the direction of the induced orbital angular momentum upon the excitation of the unpaired electron is almost parallel to the *b*-axis, resulting in a large absolute value for ε_{bb}.

The Magnetic Hyperfine Constants

The magnetic hyperfine constants (a_F and T) of the two conformers are small since the unpaired electron is mainly located on the terminal oxygen atom of the COO moiety where the spin density on the chlorine atom is smaller than 1%. The small negative Fermi contact constants of the chlorine nucleus in both conformers could be rationalized by the spin polarization effect of the Cl–C bond from the unpaired electron on the central carbon atom. This contrasts with the case of the ClSO radicals, where some amount of the unpaired electron distributed in the out-of-plane π-orbital on chlorine and the spin polarization effect of the Cl–S sigma bond results in a small positive Fermi contact constant.[12]

For the dipolar interaction constants, a radical with an unpaired electron in the out-of-plane π radical usually satisfies a ratio T_{aa}:T_{bb}:T_{cc} = –2/5:–2/5:4/5.[23] However, both the *trans*- and *cis*-ClC(O)OO radicals do not follow this relation due to the very weak interaction between the unpaired electron on the terminal oxygen nucleus and the Cl nuclear spin. The experimental results indicates that the Fermi contact constants and the dipolar interaction constants satisfy the ratio of the magnetic moments of the two isotopes 0.82:0.68[18] for the two conformers and their ^{37}Cl isotopologues.

Quadrupole Coupling Constants

The quadrupole coupling constants of the *trans*-^{35}ClC(O)OO and ^{37}ClC(O)OO radicals satisfy the ratio of the quadrupole moment of the two isotopes, 8.24:6.49,[18] while in the case of the *cis*-ClC(O)OO radical, the constants do not agree with this relation. This discrepancy is due to a small change of the molecular axes between the two chlorine isotopologues. For *trans*-ClC(O)OO, *ab initio* calculations showed that the angles between the *a*-axis and the Cl–C bond are 21.7°and 21.3° for the ^{35}Cl and ^{37}Cl isotopologues, respectively. On the other hand, the angles for the *cis*-^{35}ClC(O)OO and ^{37}ClC(O)OO radicals are 54.8° and 50.8°. The 4° difference indicates that the quadrupole coupling constants projected to the two different molecular axes are quite different for the *cis*-ClC(O)OO isotopologues and direct comparison becomes meaningless.

By diagonalizing the fitted quadrupole coupling tensor as shown in **Table 3**, the rotational angle of the quadrupole interaction tensor between the *a*-axis and the *x*-axis in the principal axis system of the tensor is 20.8° and 51.5° for *trans*-^{35}ClC(O)OO and *cis*-^{35}ClC(O)OO, which are close to the angles between the *a*-axis and the Cl–C bond. This suggests that the principal axes of the quadrupole interactions are directing almost toward the Cl–C bond. The values for the principal axis system are almost axially symmetric, *i. e.* $\chi_{xx} \approx -2\chi_{yy} \approx -2\chi_{zz}$.[23] Furthermore the ratios of the principal axis system values for the two isotopologues of *cis*-ClC(O)OO satisfy the expected ratio for the quadrupole moments.

Since the *x*-axis lies close to the Cl–C bond, the ionic character (i_c) of the Cl–C bond can be calculated from χ_{xx} as below.

$$i_c = 1 + \frac{\chi_{xx}}{eQq_{n10}},\ eQq_{n10} = 109.74 \text{ MHz for } ^{35}\text{Cl}.$$

Where, eQq_{n10} is the coupling constant of an atomic *p* electron in the orbital ψ_{n10}. The χ_{xx} of the *trans*-ClC(O)OO and *cis*-ClC(O)OO radicals are –72.39 and –73.78 MHz as

shown in **Table 3**. The ionic characters of the Cl–C bond are thus 0.34 and 0.33 for *trans*-^{35}ClC(O)OO and *cis*-^{35}ClC(O)OO, respectively, suggesting that the Cl–C bonds possess stronger covalent character in both conformers.

Insights from the Molecular Geometry

With very good agreement between the experimental results and the theoretical predictions for the molecular constants, we believe that the calculated geometries of the two conformers of the ClC(O)OO radical are very close to the true values. The O–O bond lengths of *trans*- and *cis*-^{35}ClC(O)OO are 1.326 Å and 1.318 Å, respectively. These bond length are similar to the O–O bond length of the HOO radical (1.329 Å)[24] and lie between the bond lengths of O_2 (1.208 Å) and H_2O_2 (1.475 Å),[25] suggesting that the O–O bonds of the ClC(O)OO radicals have similar reactivity as those of typical peroxyl radicals. The C=O bond lengths are 1.174 Å and 1.178 Å for the *trans*-ClC(O)OO and *cis*-ClC(O)OO conformers, respectively, which are close to the C=O bond of Cl_2CO (1.177 Å)[26] This fact indicates that the unpaired electron barely occupies the CO moiety of the ClC(O)OO radicals and suggests that the CO moiety is not the reactive center toward other species. Thus, it is possible to say the ClC(O)OO radical is a -ClCO derivative of the HOO radical.

Conclusions

Pure rotational spectra of both *trans*-ClC(O)OO and *cis*-ClC(O)O conformers, and their ^{35}Cl/^{37}Cl isotopologues were observed using an FTMW spectrometer under supersonic expansion. The observed fine and hyperfine splittings were well-assigned and the molecular constants, including the electron spin-rotation constants, the Fermi contact constant, the dipolar interaction constants, the quadrupole coupling constants and the centrifugal distortion constants were determined precisely.

The electron spin-rotation constants and the hyperfine constants agree well with the molecular orbital picture that the unpaired electron mainly occupies the out-of-plane p_c orbital of the terminal oxygen atom of the COO moiety with a small distribution to the adjacent oxygen atom, making the terminal oxygen atom the reactive center with other species.

We also found that the C=O bond lengths of ClC(O)OO are very close to that of phosgene, indicating the unpaired electron is localized on the terminal oxygen and has little effect on the ClC(O) moiety. Indeed, the Cl–C bonds in the ClC(O) moiety have

large covalent characters for both *cis*- and *trans*-conformers, suggesting that the ClC(O) moiety possesses a small reactivity with other species in the gas phase. However, the reactivity with alkaline species, e.g. NH_3, could still be strong because alkaline species tend to donate the lone pair electron to the C=O π anti-bonding orbital, especially to the central carbon.

The hyperfine structures of the $^{35}Cl/^{37}Cl$ isotopologues of *trans*-ClC(O)OO are similar; the values are proportional to the ratios of the magnetic moment and the quadrupole moment of the $^{35}Cl/^{37}Cl$ nuclei. However, in the case of the isotopologues of *cis* -ClC(O)OO, clear differences have been observed for their quadrupole coupling constants, which was attributed to the difference of the angles between the principal axes of the quadrupole tensor and the inertia axes.

Supporting Materials

The Supporting Material, which contains the transition frequencies and the assignments of all the observed transitions, is available free of charge at the journal website.

Author contributions

Ching-Hua Chang: Data curation, Formal Analysis, Investigation, Writing – review & editing. Wen Chao: Conceptualization. Cheng-Hua Tsai: Formal Analysis, Investigation. Mitchio Okumura: Conceptualization, Writing – review. Frank A. F. Winiberg: Conceptualization, Writing – review. Yasuki Endo: Conceptualization, Data curation, Formal Analysis, Funding acquisition, Methodology, Software, Writing – review & editing.

Conflicts of Interest

The authors declare no competing financial interest.

ORCID

Ching-Hua Chang. https://orcid.org/0000-0002-2008-8439
Yasuki Endo. https://orcid.org/0000-0002-8660-6729

Acknowledgements

The research was supported by the National Science and Technology Council of Taiwan (grants MOST108-2113-M-009-025, MOST109-2113-M-009-024). The work of WC and FW was supported in part by Jet Propulsion Laboratory, California Institute of Technology, under a contract with the National Aeronautics and Space Administration (80NM0018D0004). The authors thank Prof. Yuan-Pern Lee for sharing necessary lab supplies

References

1. J. G. O'Rourke, C. F. Wilson, M. E. Borrelli, P. K. Byrne, C. Dumoulin, R. Ghail, A. J. P. Gülcher, S. A. Jacobson, O. Korablev, T. Spohn, M. J. Way, M. Weller and F. Westall, Venus, the Planet: Introduction to the Evolution of Earth's Sister Planet, *Space Sci. Rev.*, 2023, **219**, 10.
2. F. Westall, D. Höning, G. Avice, D. Gentry, T. Gerya, C. Gillmann, N. Izenberg, M. J. Way and C. Wilson, The Habitability of Venus, *Space Sci. Rev.*, 2023, **219**, 17.
3. T. Widemann, S. E. Smrekar, J. B. Garvin, A. G. Straume-Lindner, A. C. Ocampo, M. D. Schulte, T. Voirin, S. Hensley, M. D. Dyar, J. L. Whitten, D. C. Nunes, S. A. Getty, G. N. Arney, N. M. Johnson, E. Kohler, T. Spohn, J. G. O'Rourke, C. F. Wilson, M. J. Way, C. Ostberg, F. Westall, D. Höning, S. Jacobson, A. Salvador, G. Avice, D. Breuer, L. Carter, M. S. Gilmore, R. Ghail, J. Helbert, P. Byrne, A. R. Santos, R. R. Herrick, N. Izenberg, E. Marcq, T. Rolf, M. Weller, C. Gillmann, O. Korablev, L. Zelenyi, L. Zasova, D. Gorinov, G. Seth, C. V. N. Rao and N. Desai, Venus Evolution Through Time: Key Science Questions, Selected Mission Concepts and Future Investigations, *Space Sci. Rev.*, 2023, **219**, 56.
4. F. P. Mills and M. Allen, A review of selected issues concerning the chemistry in Venus' middle atmosphere, *Planet. Space Sci.*, 2007, **55**, 1729-1740.
5. C. J. Bierson and X. Zhang, Chemical Cycling in the Venusian Atmosphere: A Full Photochemical Model From the Surface to 110 km, *J. Geophys. Res.: Planets*, 2020, **125**, E006159.
6. F. P. Mills, A spectroscopic search for molecular oxygen in the Venus middle atmosphere, *J. Geophys. Res.: Planets*, 1999, **104**, 30757-30763.
7. G. Piccioni, L. Zasova, A. Migliorini, P. Drossart, A. Shakun, A. García Muñoz, F. P. Mills and A. Cardesin-Moinelo, Near-IR oxygen nightglow observed by VIRTIS in the Venus upper atmosphere, *J. Geophys. Res.: Planets*, 2009, **114**, E00B38.
8. W. B. DeMore and Y. L. Yung, Catalytic Processes in the Atmospheres of Earth and Venus, *Science*, 1982, **217**, 1209-1213.
9. X. Zhang, M. C. Liang, F. P. Mills, D. A. Belyaev and Y. L. Yung, Sulfur

chemistry in the middle atmosphere of Venus, *Icarus*, 2012, **217**, 714-739.

10. B. J. Sandor and R. Todd Clancy, First measurements of ClO in the Venus atmosphere – Altitude dependence and temporal variation, *Icarus*, 2018, **313**, 15-24.
11. Y. L. Yung and W. B. DeMore, *Photochemistry of planetary atmospheres*, Oxford University Press, New York, 1999.
12. C. H. Chang, C. H. Tsai, Y. T. Liu and Y. Endo, Fourier-transform microwave spectroscopy of the ClSO radical, *Phys. Chem. Chem. Phys.*, 2024, **26**, 4922-4928.
13. J. S. Francisco and I. H. Williams, Theoretical characterization of formylperoxy and (haloformyl)peroxy radicals, *J. Phys. Chem.*, 1988, **92**, 5347-5352.
14. H. Pernice, P. Garcia, H. Willner, J. S. Francisco, F. P. Mills, M. Allen and Y. L. Yung, Laboratory evidence for a key intermediate in the Venus atmosphere: Peroxychloroformyl radical, *Proc. Natl. Acad. Sci. U.S.A.*, 2004, **101**, 14007-14010.
15. B. Behera and Y.-P. Lee, Infrared spectra of gaseous peroxychloroformyl radical ClC(O)OO: A key intermediate in the conversion of CO to CO2 in the Venus atmosphere, *J. Mol. Spectrosc.*, 2023, **393**, 111771.
16. H.-J. Werner, P. J. Knowles, G. Knizia, F. R.Manby, M. Schütz, P. Celani, W. Györffy, D. Kats, T. Korona, R. Lindh, A. Mitrushenkov, G. Rauhut, K. R. Shamasundar, T. B. Adler, R. D. Amos, S. J. Bennie, A. Bernhardsson, A. Berning, D. L. Cooper, M. J. O. Deegan, A. J. Dobbyn, F. Eckert, E. Goll, C. Hampel, A. Hesselmann, G. Hetzer, T. Hrenar, G. Jansen, C. Köppl, S. J. R. Lee, Y. Liu, A. W. Lloyd, Q. Ma, R. A. Mata, A. J. May, S. J.McNicholas, W. Meyer, T. F.Miller, M. E. M. III, A. Nicklass, D. P. O'Neill, P. Palmieri, D. Peng, K. Pflüger, R. Pitzer, M. Reiher, T. Shiozaki, H. Stoll, A. J. Stone, R. Tarroni, T. Thorsteinsson, M. Wang and M. Welborn, 2022.1, a package of ab initio programs edn., 2022. see *http://www.molpro.net*.
17. M. J. Frisch, G. W. Trucks, H. B. Schlegel, G. E. Scuseria, M. A. Robb, J. R. Cheeseman, G. Scalmani, V. Barone, G. A. Petersson, H. Nakatsuji, X. Li, M. Caricato, A. V. Marenich, J. Bloino, B. G. Janesko, R. Gomperts, B. Mennucci, H. P. Hratchian, J. V. Ortiz, A. F. Izmaylov, J. L. Sonnenberg, Williams, F. Ding, F. Lipparini, F. Egidi, J. Goings, B. Peng, A. Petrone, T. Henderson, D. Ranasinghe, V. G. Zakrzewski, J. Gao, N. Rega, G. Zheng, W. Liang, M. Hada, M. Ehara, K. Toyota, R. Fukuda, J. Hasegawa, M. Ishida, T. Nakajima, Y. Honda, O. Kitao, H. Nakai, T. Vreven, K. Throssell, J. A. Montgomery Jr., J. E. Peralta, F. Ogliaro, M. J. Bearpark, J. J. Heyd, E. N. Brothers, K. N. Kudin, V. N. Staroverov, T. A. Keith, R. Kobayashi, J. Normand, K. Raghavachari, A.

P. Rendell, J. C. Burant, S. S. Iyengar, J. Tomasi, M. Cossi, J. M. Millam, M. Klene, C. Adamo, R. Cammi, J. W. Ochterski, R. L. Martin, K. Morokuma, O. Farkas, J. B. Foresman and D. J. Fox, Gaussian Wallingford, CT2016.

18. N. J. Stone, Table of nuclear magnetic dipole and electric quadrupole moments, *Atomic Data and Nuclear Data Tables*, 2005, **90**, 75-176.
19. C. Cabezas, J.-C. Guillemin and Y. Endo, Fourier-transform microwave spectroscopy of a halogen substituted Criegee intermediate ClCHOO, *J. Chem. Phys.*, 2016, **145**, 184304.
20. C. H. Chang, C. H. Tsai, and Y. Endo, to be published.
21. J. M. Nicovich, K. D. Kreutter and P. H. Wine, Kinetics and thermochemistry of ClCO formation from the Cl+CO association reaction, *J. Chem. Phys.*, 1990, **92**, 3539-3544.
22. K. Suma, Y. Sumiyoshi, Y. Endo, S. Enami, S. Aloisio, S. Hashimoto, M. Kawasaki, S. Nishida and Y. Matsumi, Equilibrium Constants of the Reaction of Cl with O2 in the Formation of ClOO, *J. Phys. Chem. A*, 2004, **108**, 8096-8099.
23. E. Hirota *et al*., *High-resolution spectroscopy of transient molecules*, Springer-Verlag, Berlin ; New York, 1985.
24. A. Charo and F. C. De Lucia, The millimeter and submillimeter spectrum of HO2: The effects of unpaired electronic spin in a light asymmetric rotor, *J. Mol. Spectrosc.*, 1982, **94**, 426-436.
25. K. P. Huber and G. Herzberg, *Molecular Spectra and Molecular Structure IV. Constants of Diatomic Molecules*, Van Nostrand Reinhold, New York, 1979.
26. K. Kuchitsu, *Structure of Free Polyatomic Molecules*, Springer Berlin, Heidelberg1998.

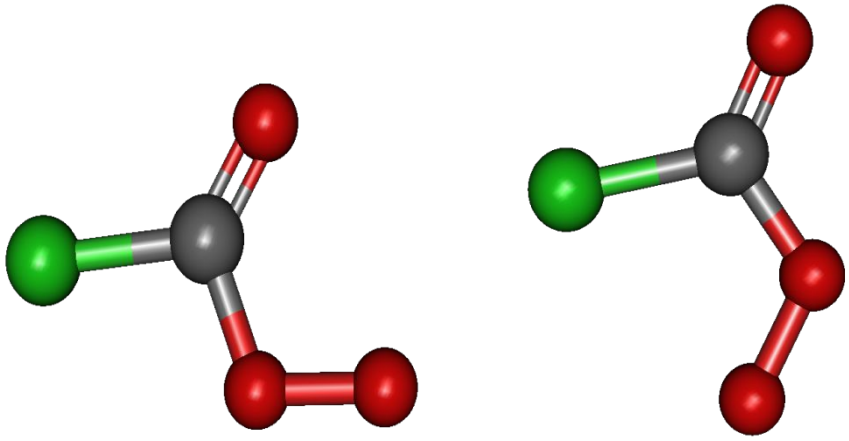

Fig. 1. Schematic pictures of the two conformers, (left) *trans*-ClC(O)OO and (right) *cis*-ClC(O)OO. The geometries were optimized at RCCSD(T)-F12A/cc-pVTZ-f12 with the *cis*-conformer about 2.65 kJ mol^{-1} higher than the *trans*- conformer with the zero-point energy corrections at RCCSD(T)/cc-pVTZ.

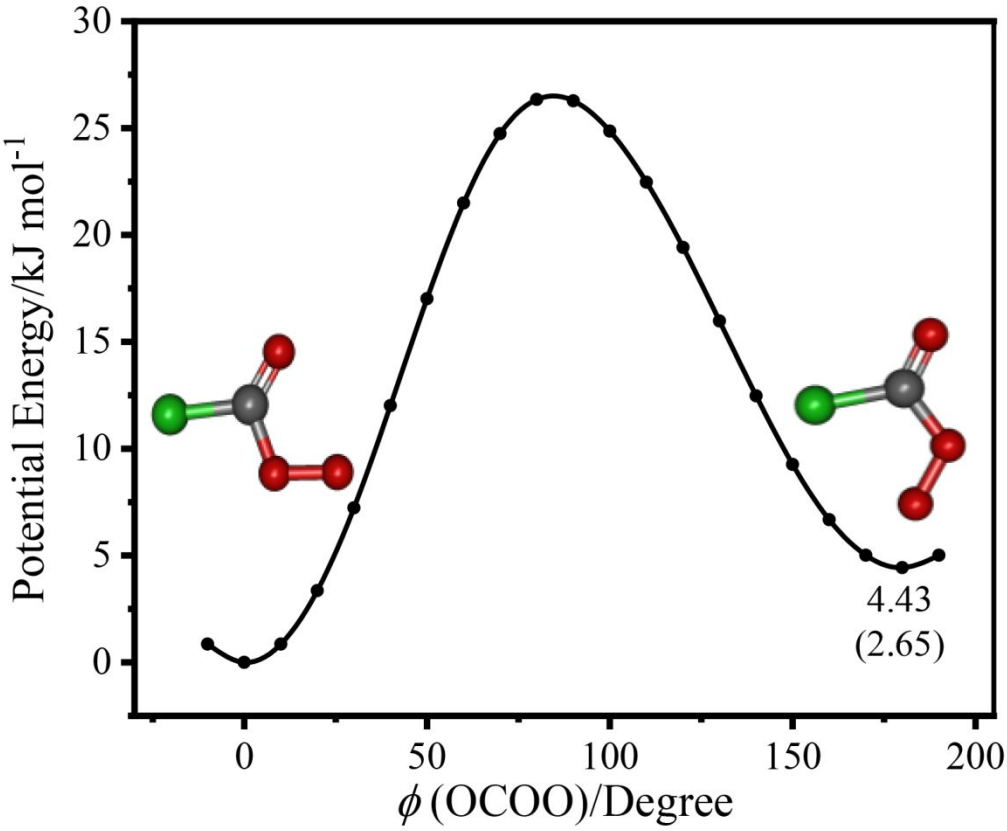

Fig. 2. The Potential Energy Surface rotating the OCOO dihedral angle, ϕ(ClCOO), calculated at the RCCSD(T)/cc-pVTZ level of theory. The energy shown in the parenthesis was calculated at the RCCSD(T)-F12A/cc-pVTZ-f12 level of theory with the zero-point energy correction calculated at RCCSD(T)/cc-pVTZ.

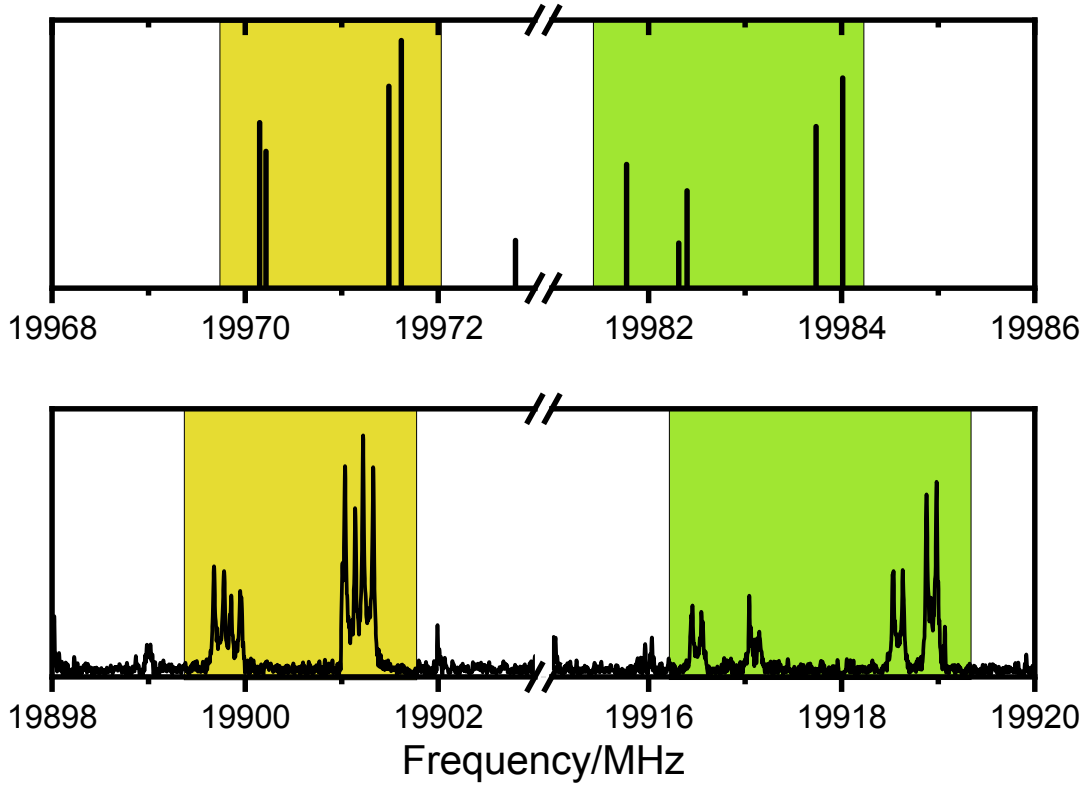

Fig. 3. Representative microwave spectrum of the 4_{04}-3_{03} transition of the *trans*-^{35}ClC(O)OO radical. The upper panel shows the predicted fine and hyperfine structures. The lower panel shows the experimental spectrum. The predictions are very close to the experimental result with only the 70 MHz frequency difference. The two colored regions mark the splitting due to the electron spin-rotation interaction. In each region, four transitions were observed due to the hyperfine splitting. Each hyperfine component has a doublet line shape due to Doppler splitting.

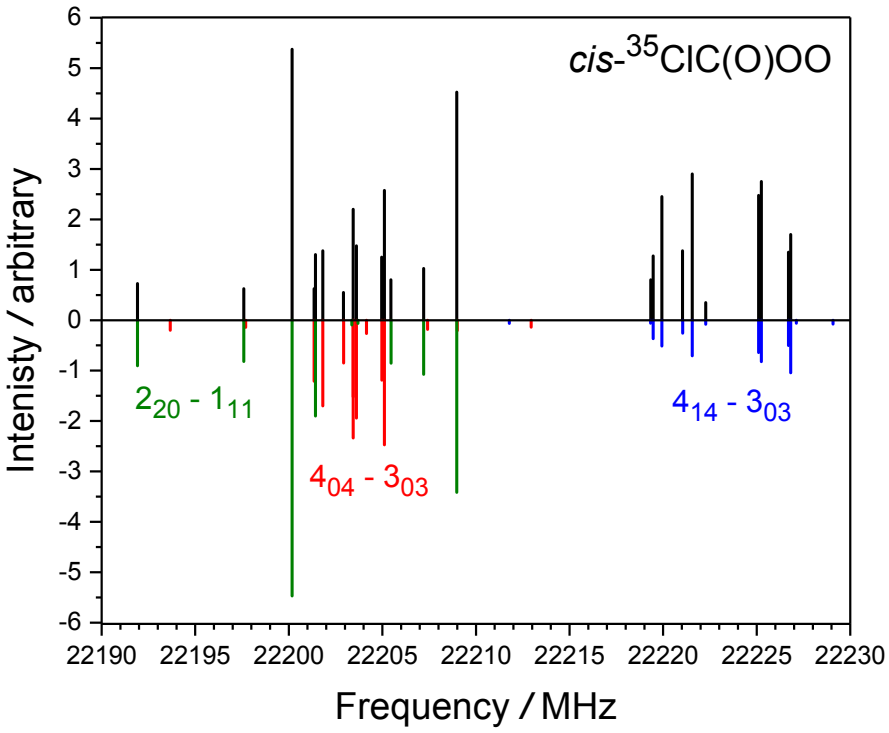

Fig. 4. The observed spectral pattern of the *cis*-^{35}ClC(O)OO radical in the 22190–22230 MHz region. The upward black sticks are the observed spectral lines. The downward sticks are the predictions of 4_{04}-3_{03} (red), 2_{20}-1_{11} (green) and 4_{14}-3_{03} (blue) transitions.

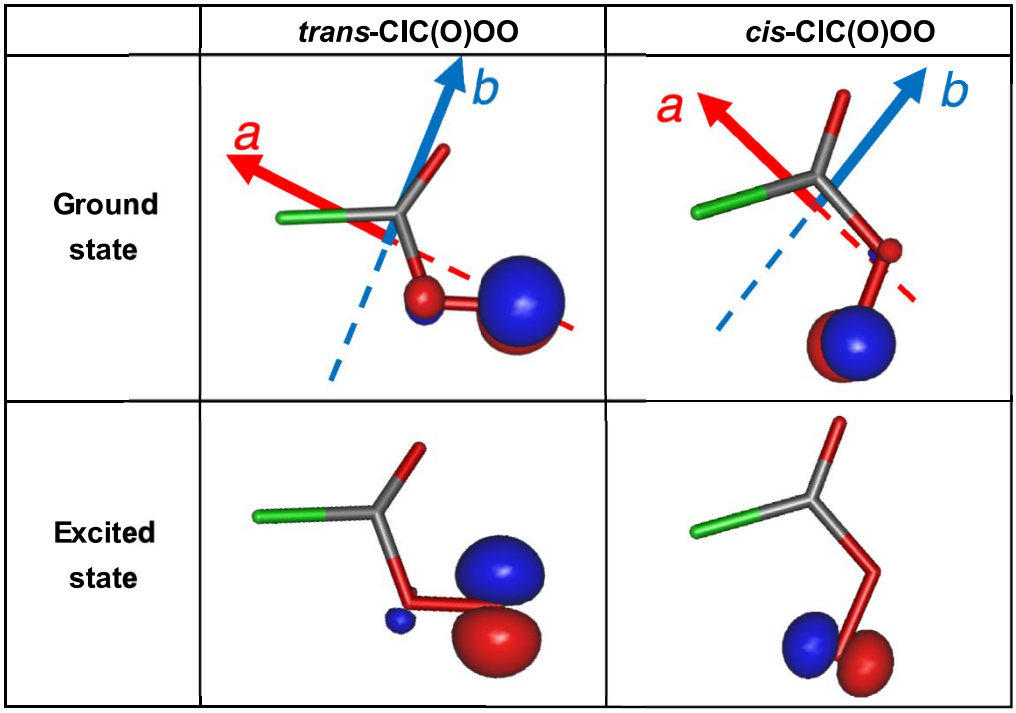

Fig. 5. The singly occupied molecular orbitals of each conformer in its electronic ground state and the first excited state. The geometries of the radicals were optimized using the Molpro program package at the RCCSD(T)-F12A/cc-p-VTZ-f12 level of theory.

Table 1. Molecular constants of ^{35}ClC(O)OO. (in MHz)

	trans-^{35}ClC(O)OO		*cis*-^{35}ClC(O)OO	
	Experimetal	Theoretical[a]	Experimetal	Theoretical
$\|\mu_a\|$ / Debye		0.91		0.27
$\|\mu_b\|$ / Debye		1.13		1.83
$\|\mu_c\|$ / Debye		0.00		0.00
E / Hartree		-723.16487		-723.16382
ΔE / kJ mol^{-1}		0.00[b]		2.65
A	9845.42070(44)	9899.27	5620.75213(56)	5629.72
B	2864.08677(19)	2871.94	4383.39228(58)	4406.68
C	2217.79780(15)	2226.11	2461.93103(21)	2471.84
Δ_N / 10^{-3}	0.3843(15)	0.38	1.857(23)	3.11
Δ_{NK} /10^{-3}	1.073(36)	1.16	-3.916(87)	-7.77
Δ_K / 10^{-3}	16.59[c]	16.59	4.94	4.94
δ_N / 10^{-3}	0.0962(14)	0.097	0.795(11)	-0.21
δ_K / 10^{-3}	1.688	1.688	0.644(56)	-5.00
ε_{aa}	-943.0312(24)	-628.33	-119.33402(88)	-98.78
ε_{bb}	-31.4980(14)	-28.48	-315.08782(77)	-214.60
ε_{cc}	-0.90782(91)	1.26	-0.70265(57)	1.97
ε_{ab}	48.6318(39)	26.60	126.509(18)	82.41
a_F (Cl)	-0.6353(25)	-0.23	-1.46513(82)	-1.49
T_{aa} (Cl)	-2.5957(43)	-3.09	0.8961(14)	1.27
T_{bb} (Cl)	-0.9539(33)	-1.63	-0.0310(13)	0.09
T_{ab} (Cl)	-0.113(17)	-0.38	-0.329(14)	-0.29
χ_{aa} (Cl)	-57.6002(70)	-54.50	-0.0084(26)	-0.089
χ_{bb} (Cl)	29.3558(65)	29.34	-27.1927(25)	-24.26
χ_{ab} (Cl)	38.64(14)	36.44	-58.626(51)	-56.53
C_{aa} (Cl) / 10^{-3}	1.6	1.6	1.9	1.9
C_{bb} (Cl) / 10^{-3}	1.3	1.3	1.3	1.3
C_{cc} (Cl) / 10^{-3}	0.9	0.9	0.8	0.8
σ_{fit} / 10^{-3}	2.5		2.0	

[a]The rotational constants were derived from the geometry calculated at the RCCSD(T)-f12a/cc-pVTZ-f12 level of theory. Other parameters were calculated at the B3LYP/cc-pVTZ level of theory at the optimized structures calculated by the Molpro program.

[b]The zero-point energies of the two conformers were corrected at the RCCSD(T)/cc-pVTZ level of theory by the Molpro program.

[c]The values in parentheses denote one standard deviation of the fit and apply to the last digits. The values without uncertainty are kept fixed to those obtained theoretically.

Table 2. Molecular constants of ^{37}ClC(O)OO. (in MHz)

	trans-^{37}ClC(O)OO		*cis*-^{37}ClC(O)OO	
	Experimetal	Scaled[a]	Experimetal	Scaled
A	9816.4384(15)	9814.05	5554.96351(73)	5554.45
B	2787.75518(16)	2787.11	4292.30194(33)	4290.57
C	2170.32793(30)	2169.77	2420.49990(38)	2419.89
Δ_N / 10^{-3}	0.3708(74)	0.36	1.934(18)	3.00
Δ_{NK} /10^{-3}	0.970(85)	1.07	-4.338(74)	-7.53
Δ_K / 10^{-3}	16.79[b]	16.79	4.80	4.80
δ_N / 10^{-3}	0.09	0.09	-0.22	-0.22
δ_K / 10^{-3}	1.62	1.62	1.18(16)	-4.71
ε_{aa}	-941.6597(71)	-941.17	-101.3454(23)	-104.91
ε_{bb}	-30.2644(22)	-30.45	-321.3447(31)	-320.76
ε_{cc}	-0.8966(15)	-0.88	-0.6934(10)	-0.69
ε_{ab}	45.219(61)	43.92	108.179(56)	108.77
a_F (Cl)	-0.5274(17)	-0.56	-1.2228(41)	-1.22
T_{aa} (Cl)	-2.1510(47)	-2.15	-0.6992(52)	0.75
T_{bb} (Cl)	-0.8023(55)	-0.79	0.0132(31)	-0.03
T_{ab} (Cl)	-0.12*	-0.09	-0.429(61)	-0.27
χ_{aa} (Cl)	-45.822(11)	-45.39	-5.7959(86)	-0.01
χ_{bb} (Cl)	23.5516(77)	23.14	-15.6387(71)	-21.43
χ_{ab} (Cl)	30.49(38)	30.45	-47.23(17)	7.09
C_{aa} (Cl) / 10^{-3}	1.3	1.3	1.5	1.5
C_{bb} (Cl) / 10^{-3}	1.0	1.0	1.1	1.1
C_{cc} (Cl) / 10^{-3}	0.7	0.7	0.7	0.7
σ_{fit} / 10^{-3}	1.5		1.9	

[a]All parameters were scaled with the experimental and calculated values of ^{35}ClC(O)OO, and the ratios of the magnetic moments, and the quadrupole moments of the isotopes for the hyperfine constants.

[b]The values in parentheses denote one standard deviation of the fit and apply to the last digits. The values without uncertainty are kept fixed to those obtained theoretically.

Table 3. Inertial axis and principal axis values of T and χ tensors of ClC(O)OO. (in MHz)

	trans-^{35}ClC(O)OO	*trans*-^{37}ClC(O)OO	*cis*-^{35}ClC(O)OO	*cis*-^{37}ClC(O)OO
a_F(Cl)	-0.64	-0.53	-1.46	-1.22
T_{aa}(Cl)	-2.60	-2.15	0.90	-0.70
T_{bb}(Cl)	-0.95	-0.80	-0.03	0.01
T_{ab}(Cl)	-0.11	-0.12	-0.33	-0.43
θ_T[a]/degree	3.80	5.04	17.68	25.23
T_{xx}(Cl)	-2.61	-2.16	-0.14	0.90
T_{yy}(Cl)	-0.94	-0.79	1.01	0.21
T_{zz}(Cl)	3.55	2.95	-0.87	-1.11
χ_{aa}(Cl)	-57.60	-45.82	-0.01	-5.80
χ_{bb}(Cl)	29.36	23.55	-27.19	-15.64
χ_{ab}(Cl)	38.64	30.49	-58.63	-47.23
θ_χ[b]/degree	20.81	20.66	51.53	47.97
χ_{xx}(Cl)	-72.39	-57.32	-73.78	-58.21
χ_{yy}(Cl)	44.05	35.05	46.58	36.77
χ_{zz}(Cl)	28.24	22.27	27.2	21.44

[a]The rotation angle from T_{aa} to T_{xx}, in degree.
[b]The rotation angle from χ_{aa} to χ_{xx}, in degree.

Data availability statement

for “Insights of the Peroxychloroformyl Radical ClC(O)OO via Microwave Spectrum”
by Ching-Hua Chang, Wen Chao, Cheng-Han Tsai, Mitchio Okumura, Frank A. F. Winiberg, and Yasuki Endo

All the date in the manuscript is included in the supplementary file.